Human Immunology 87 (2026) 111684

Contents lists available at ScienceDirect

Human Immunology

journal homepage: www.elsevier.com/locate/humimm

Research article

A wide proteome analysis to engineer an efficient epitope based vaccine against *Salmonella* typhi: An immunoinformatic study

Mahsa Beiranvand [a], Nemat Shams [a,*], Amin Jaydari [a], Narges Nazifi [b], Peyman Khademi [a]

[a] Faculty of Microbiology and Food Health, Department of Veterinary Medicine, Lorestan University, Iran
[b] Faculty of basic science, Department of Veterinary Medicine, Lorestan University, Iran

ARTICLE INFO

Keywords:
Recombinant Vaccine
Proteome
Salmonella Typhi
Typhoid
Immunoinformatic

ABSTRACT

Background: Typhoid fever, a potentially fatal disease caused by *Salmonella* enterica serovar Typhi, requires effective vaccines. This study aimed to design a recombinant subunit vaccine using the most immunogenic proteins from the *Salmonella* Typhi proteome.
Methods: Initially, the most antigenic proteins were selected to predict linear T-cell, B-cell, and IFN-γ epitopes. A recombinant construct incorporating these epitopes, peptide linkers, and a molecular adjuvant was designed. Comprehensive evaluation assessed physicochemical properties, solubility, secondary/tertiary structure, antigenicity, and immune stimulation potential. Molecular docking and dynamics simulations investigated binding to the TLR4/MD2 receptor complex.
Results: Seven proteins from 4322 were chosen for epitope prediction, yielding a 655-amino acid construct. Physicochemical analysis showed 40.31 % hydrophobic amino acids, an aliphatic index of 53.66, GRAVY index of −0.712, and instability index of 22.34. Structural composition was 53.53 % alpha-helix, 8.85 % extended strand, and 40.61 % random coil. Immune simulations demonstrated significant enhancement of primary/secondary humoral and cellular immune responses. The vaccine construct effectively bound the TLR4/MD2 receptor via significant hydrogen bonding (affinity: −1019.1 kcal/mol). Molecular dynamics simulations confirmed the stability of this interaction over 200 ns, demonstrating that both the vaccine candidate and receptor remained structurally stable throughout the simulation period.
Conclusion: Typhoid vaccine candidate shows immunogenic properties, robust immune responses and stable TLR4/MD2 receptor binding.

1. Introduction

Salmonella enterica serovar Typhi is a facultative intracellular pathogen that causes typhoid fever in humans (1). Typhoid fever initiates infection via ingestion of contaminated food or water, followed by invasion of the intestinal mucosa and Peyer's patches. Subsequently, the gallbladder may serve as a chronic storage site in asymptomatic carriers. This multistage disease progresses through distinct phases and presents with severe complications, including intestinal perforation, usually by the third week. Patients may recover after contracting the disease, and in another group, it may lead to the death of the patient (2). The incidence and mortality rates of typhoid fever is concerning. Previous studies have reported that the regional incidence of this disease has been observed from less than 0.1 per 100,000 cases per year in Central and Eastern Europe and Central Asia to 724.6 per 100,000 cases per year in Sub-Saharan Africa [1]. Therefore, the greatest burden of this disease is in developing countries, where it causes more than 10 million cases and 100,000 deaths [2]. Vaccination remains the most cost-effective public health intervention for infectious disease control. Typhoid fever exemplifies a major global health challenge within the category of infectious diseases, which collectively cause more than 9 million deaths annually (WHO, 2020). Nowadays, the design and production of vaccines using the immunogenic parts of pathogens has attracted the attention of researchers [3]. On the other hand, the emergence of multi-drug resistant strains of *Salmonella* Typhi has added an urgent need to produce more effective typhoid vaccines [4]. The oral Ty21a (as capsules and as a liquid suspension) and injectable Vi capsular polysaccharide vaccines are two available licensed vaccines in the world to deal with typhoid fever [5]. The Ty21a vaccine is a live attenuated vaccine, which requires 3 to 4 doses in a vaccination period because the immunity develops 10 to

* Corresponding author.
E-mail address: Shams.n@lu.ac.ir (N. Shams).

https://doi.org/10.1016/j.humimm.2026.111684
Received 26 April 2025; Received in revised form 16 December 2025; Accepted 1 February 2026
Available online 11 February 2026

14 days after receiving the third dose. Also, this vaccine needs a booster dose every 5 years, and the use of anti-malarial drugs reduces the immunogenicity of this vaccine [6]. The injectable Vi capsular polysaccharide vaccine is not immunogenic in children under 2 years old and is only licensed for use in people over 2 years old. This vaccine was 64 % effective after 21 months, dropping to 55 % 3 years after vaccination. then it is recommended that vaccination be done every 3 years to maintain protection [7]. This study used a comprehensive proteome-wide screening to identify highly immunogenic proteins of *Salmonella enterica* serovar Typhi for designing a multi-epitope subunit vaccine. This study hypothesized that a construct based on the most likely predicted epitopes of T cells, B cells, and IFN-γ, linked to a molecular adjuvant via peptide linkers, would exhibit optimal immunogenicity and physicochemical properties. Key features of this candidate vaccine were then evaluated to further validate this hypothesis.

2. Material and methods

2.1. Data collection

In this study with the aim of access to the proteome of *Salmonella* Typhi with the accession number of AE014613.1, and the amino acid sequence of HBHA protein with the accession number of NP_214989.1b the NCBI server (https://www.ncbi.nlm.nih.gov/) was used. In parallel, the pdb structure of TLR4/MD2 (Toll-like receptor 4 /myeloid differentiation factor 2) protein was retrieved from the RCSB server (https://www.rcsb.org/) using the 2Z64 ID number.

2.2. Investigating the protectiveness, allergenicity and antigenicity of the proteome

In this study, in order to evaluating antigenicity and allergenicity of proteins in the proteome, the VaxiJen (https://www.ddg-pharmfac.net/vaxijen/VaxiJen/VaxiJen.html) and AllerTOP (https://www.ddg-pharmfac.net/AllerTOP/method.html) servers were used, respectively. While using the mentioned servers, the raw sequence of proteins and peptides were submitted and the default settings of VaxiJen and AllerTOP software were employed. VaxiJen is the first server for alignment-independent prediction of protective antigens. It was developed to classify antigens based solely on the physicochemical properties of proteins without reference to sequence alignment. AllerTOP server uses the auto cross covariance (ACC) transformation method to convert protein sequences into uniform, equal-length vectors [8].

2.3. Prediction of the most epitopic region and evaluation of their toxicity

To identify optimal T-cell epitopes for MHCI and MHCII molecules, IEDB (https://tools.iedb.org/main/tcell/), ProPred (https://crdd.osdd.net/raghava/propred/) servers have been employed. These servers predicted MHCI epitopes for A01:01, A02:01, and B27:05 alleles, and MHCII epitopes for DRB101:01 and DRB1 04:01 alleles. The IEDB server utilizes Stabilized Matrix Method (SMM) and Artificial Neural Network (ANN)-based approaches for T-cell epitope prediction [9].

For B-cell epitope prediction, BepiPred-3.0 algorithm implemented in IEDB analysis resource (https://tools.iedb.org/bcell/) and ABCpred (https://crdd.osdd.net/raghava/abcpred/) have been utilized. BepiPred-3.0 employs scale-based and Hidden Markov Model (HMM) methods for linear epitope prediction and automatically excludes regions with predicted N-/O-glycosylation sites by default [10,11].

Moreover, the IFNepitope server (https://webs.iiitd.edu.in/raghava/ifnepitope/scan.php) was employed to identify regions likely recognized by IFN-γ. This server employs motif-based and Support Vector Machine (SVM)-based algorithms to discriminate IFN-γ inducing peptides [12]. Subsequently, the ToxinPred server (https://webs.iiitd.edu.in/raghava/toxinpred/design.php) assessed epitope toxicity using SVM-based algorithms.

2.4. Epitope conservation and population coverage analysis

Conservation of epitopes across *Salmonella* serovars was evaluated using BLASTP (NCBI). Epitope sequences were queried against reference proteomes of *S. Typhimurium* (LT2; NCBI: txid90371), *S. Enteritidis* (P125109; NCBI: txid59201), S. Typhi (Ty2; NCBI: txid198214)), and S. Newport (Sl254; NCBI: txid573671) using optimized parameters for short sequences (word size: 2, expect threshold: 1000).

Population coverage was calculated using the IEDB population coverage tool (https://tools.iedb.org/population/) for MHC class I (A01:01, A02:01, B27:05) and class II (DRB101:01, DRB104:01) alleles. Allele frequencies were sourced from the Allele Frequency Net Database (AFND) The selected areas/populations were East Asia, Northeast Asia, Southeast Asia, southwest Asia, Europe, east Africa, west Africa, north Africa.

2.5. Engineering and immunoinformatics evaluation of recombinant structure

Designing a recombinant immunoinformatics structure based on the best epitopes screened from the previous steps (C −terminal) along with a molecular adjuvant (HBHA molecule with accession number of P9WIP9) (N- terminal) and the most suitable rigid peptide linkers was done using CLC Main workbench software (V 5.5). In epitopic domain of this structure, the best epitopes of T-cell, then B-cell and finally INF-γ epitopes were placed respectively, which were linearly connected to each other by a rigid peptide linker. Evaluation of the antigenicity of the recombinant structure was done by the VaxiJen server.

The secondary and the tertiary structures of the mentioned structure were also evaluated. For this purpose, the SOPMA (https://npsa-pbil.ibcp.fr/cgi-bin/npsa_automat.pl?page=/NPSA/npsa_gor4.html) and I-TASSER (https://zhanggroup.org) /I-TASSER/) servers were used along with the amino acid sequence of the designed recombinant structures. Then, the best proposed I-TASSAR model was refined using the GalaxyRefine server (https://galaxy.seoklab.org/cgi-bin/submit.cgi?type = REFINE). Finally, to identify the best refined tertiary structures, Ramachandran analysis was performed for each candidate model using the VADAR server (https://vadar.wishartlab.com).

2.6. Evaluation of the recombinant structure: physicochemical characteristics, solubility, and immunogenicity

The most important physicochemical characteristics of the designed structure (such as molecular weight, isoelectric point, estimated half-life, instability index, GRAVY index and aliphatic index) as well as its solubility were investigated via the ProtParam (https://web.expasy.org/protparam/) and PEPTIDE 2.0 (https://www.peptide2.com/N_peptide_hydrophobicity_hydrophilicity.php) servers, respectively. In the following, the evaluation of the stimulation of the immune system of the recombinant designed structure was performed by the C-ImmSim server (https://kraken.iac.rm.cnr.it/C-IMMSIM/index.php). In this regard, immune simulations were performed with random seed of 12345 and volume 10. MHC class I alleles were HLA-A0101, HLA-A0102 and HLA-B2705. HLA-DRB1_0101 and HLA-DRB1_0102 alleles were used for MHC class II. Vaccinations (LPS-free, adjuvant 100 units, antigen count matched to epitopes) were administered on days 1, 28, and 59. For using this server, the amino acid sequences of the recombinant structure were submitted in FASTA format.

2.7. Molecular docking

Protein-protein docking between the HBHA domain (N-terminal region of the recombinant epitope-based construct) as ligand and the TLR4/MD2 complex as receptor was performed using the ClusPro v2.0 automated server (https://cluspro.bu.edu/login.php). ClusPro employs Piper, an FFT-based rigid-body docking algorithm that systematically

samples ligand orientations through rotational and translational searches on a grid centered on the receptor. The algorithm identifies poses with the most favorable binding energies and discards unstable configurations. Subsequently, the server clusters the remaining poses based on structural similarity, using a 9 Å root-mean-square deviation (RMSD) cutoff for alpha-carbon atoms. The resulting top-scoring cluster centroid was selected as the representative docking pose. Hydrogen bonding interactions within this complex were analyzed using LigPlot + v1.4.5 to generate 2D interaction diagrams, while PyMOL v1.3 was used for 3D structural visualization of the binding interface and key interacting residues.

2.8. Molecular dynamics

Molecular dynamics (MD) simulations were performed using GROMACS 5.1.4 to evaluate the stability of the engineered vaccine construct complexed with TLR4/MD2. Initial structures were preprocessed with pdb2gmx to add hydrogen atoms. The CHARMM36 force field and TIP3P water model were applied to all systems. Each system was solvated in a dodecahedral water box, maintaining a minimum 1.0 nm distance between the solute and box edges. Ions were added to neutralize system charge. Energy minimization was performed using the steepest descent algorithm. Subsequently, two equilibration phases were conducted: NVT (constant Number of particles, Volume, and Temperature) and NPT (constant Number of particles, Pressure, and Temperature). Production MD simulations were run for 200 ns in the NPT ensemble at 310 K and 1 bar pressure, using a 2 fs time step. Bond lengths were constrained with the LINCS algorithm, and periodic boundary conditions were applied. System stability was assessed by calculating root mean square deviation (RMSD), root mean square fluctuation (RMSF), and radius of gyration (Rg). Binding free energy (ΔTOTAL) was computed using the MM/PBSA (Molecular Mechanics Poisson-Boltzmann Surface Area) method (gmx_mmpbsa tool) on the last 50 ns of the trajectory (sampling interval: 2 ps). Energy contributions were decomposed into gas-phase energy (ΔGGAS), polar solvation energy (ΔGPOL), and nonpolar solvation energy (ΔGNP).

3. Results

3.1. Whole proteome mining of the Salmonella Typhi and immunological assessments

The amino acid sequences of 4322 proteins constituting the *Salmonella* Typhi proteome were extracted from the NCBI server. Initially, antigenic proteins were identified using the VaxiJen server with its default threshold. Proteins classified as non-antigens were excluded from further analysis. The remaining proteins were then screened for allergenicity using the AllerTop server. Proteins predicted as allergens were removed, leaving 200 candidates. These 200 proteins underwent a second VaxiJen evaluation using a higher threshold (antigenicity ≥ 1.5). This stringent selection yielded 19 proteins with the highest antigenicity scores (accession numbers: AAO68071.1, AAO68335.1, AAO69049.1, AAO69076.1, AAO69118.1, AAO69225.1, AAO69267.1, AAO69385.1, AAO69399.1, AAO69422.1, AAO69489.1, AAO69580.1, AAO69743.1, AAO69748.1, AAO70162.1, AAO70192.1, AAO70695.1, AAO70705.1, AAO71551.1). To eliminate redundancy, sequences of these 19 proteins were aligned using the UniProt server's align procedure. Among protein pairs exhibiting > 80 % sequence similarity, the protein with the lower antigenicity score was discarded. Additionally, proteins shorter than 40 amino acids were removed. This filtering step eliminated 12 proteins (accession numbers: AAO68335.1, AAO69076.1, AAO69118.1, AAO69225.1, AAO69267.1, AAO69385.1, AAO69422.1, AAO69489.1, AAO69580.1, AAO69748.1, AAO70192.1, AAO70705.1). The characteristics of the final 7 remaining proteins are presented in Table 1.

3.2. Prediction of immunogenic epitopes and evaluation of their toxicity potential

Seven proteins screened from the previous phase entered the epitope mapping process to identify candidates capable of stimulating cellular (MHC class I/II-restricted) and humoral (B-cell-mediated) immunity. Using the immunoinformatics servers, the epitopes that showed superior prediction scores for MHC-I, MHC-II, B cell epitopes were selected. Simultaneously, IFN-γ-inducing epitopes, which are critical mediators of cellular immunity, predicted using the IFNepitope server, and selection was based on the highest-scoring candidates (Table 2). All epitopes were validated for antigenicity (VaxiJen server) and non-toxicity (ToxinPred server) before being used in the design of recombinant vaccine constructs.

Furthermore, it should be noted that, BLASTP analysis revealed exceptional evolutionary conservation of MHCI epitopes across *Salmonella* serovars. Twenty-five of 28 MHCI epitopes (89.3 %) exhibited 100 % sequence identity across all tested serovars (*S. Typhimurium, S. Enteritidis, S. Typhi, S. Newport*). Only three epitopes (GLSSAAFAA, KQAEEAAKL, RRLPKFGFTSR) demonstrated moderate variability (80–90 % identity) in *S. Typhimurium* strains. All alignments demonstrated statistically significant E-values (≤ 1.0) (Table 3). In this study, the analysis of population coverage for the MHC alleles revealed that the selected alleles had highest overage in Europe (87.97 %) West Africa (74.89 %) and Southwest Asia (73.82 %), while South Africa demonstrated significantly lower coverage (17.41 %). East Africa (67.72 %), North Africa (66.94 %) and Central Africa (53.32 %) also presented moderate coverage (Table 4).

Table 1
Characteristics of the most antigenic proteins screened from scanning the proteome of *Salmonella* Typhi.

NCBI acc.no	UniProt ID	UniProt name	Protein name	Gene name	Organism	Length (aa)
AAO68071.1	Q8Z4Q7	Q8Z4Q7_SALTI	Inner membrane protein	t0352	*Salmonella* Typhi	86
AAO69049.1	Q93MH4	ASR_SALTI	Acid shock protein	asr	*Salmonella* Typhi	83
AAO69399.1	P0A1E6	CSGA_SALTI	Major curlin subunit, Fimbrin SEF17	csgA	*Salmonella* Typhi	151
AAO70162.1	Q93IS5	Q93IS5_SALTI	Hcp1 family type VI secretion system effector, Type VI secretion system tube protein Hc	STY0302	*Salmonella* Typhi	161
AAO70695.1	Q8XG14	Q8XG14_SALTI	DUF805 domain-containing protein, Membrane protein	STY3414,	*Salmonella* Typhi	121
AAO71551	P66074	RL15_SALTI	Large ribosomal subunit protein uL15, 50S ribosomal protein L15	rplO	*Salmonella* Typhi	144
AAO69743.1	Q8Z8C1	Q8Z8C1_SALTI	Cell envelope integrity protein TolA, TolA protein	tolA	*Salmonella* Typhi	376

Table 2
Comprehensive list of specialized epitopes.

Accession Number	Epitope Sequence	Type	Antigenicity	Toxicity
AAO68071.1	FSHTVGLTY	MHCI	0.6238	Non-toxic
	MRFFFILMVLPGADR	MHCII	1.3738	Non-toxic
	KEEEKTDKQYDTGHAS	B-cell	1.4232	Non-toxic
	GSGWVLQRYYQGEER	IFN-γ	0.7250	Non-toxic
AAO69049.1	GLSSAAFAA	MHCI	0.6640	Non-toxic
	SAAFAAETATPAKTA	MHCII	0.6131	Non-toxic
	EQKAQAAKKHQKKDGK	B-cell	1.8015	Non-toxic
	GIKMKKVLALVVAAA	IFN-γ	0.5741	Non-toxic
AAO69399.1	NSDITVGQY	MHCI	1.1410	Non-toxic
	TQNGFRNNATIDQWNA	MHCII	0.5002	Non-toxic
	SETTITQSGYGNGADV	B-cell	1.6164	Non-toxic
	GGGGNHNGGGNSSGP	IFN-γ	3.49.4	Non-toxic
AAO69743.1	KQAEEAAKL	MHCI	0.9642	Non-toxic
	VQQYNRQQDQQASAR	MHCII	1.4253	Non-toxic
	DEHIEASAGGGGGSAI	B-cell	2.6533	Non-toxic
	AAAEAKKKAEAEAAK	IFN-γ	1.4203	Non-toxic
AAO70162.1	VTNLDFDHY	MHCI	0.7121	Non-toxic
	RWNIHQESTMHAGSG	MHCII	1.2464	Non-toxic
	GGTITAGYDFKANKEI	B-cell	1.3902	Non-toxic
	STMHAGSGLGSGKVS	IFN-γ	1.3951	Non-toxic
AAO70695.1	NRFGPDPKRF	MHCI	0.6670	Non-toxic
	IIAFNCQNGTPGDNR	MHCII	1.3708	Non-toxic
	NCQNGTPGDNRFGPDP	B-cell	1.5570	Non-toxic
	LLLLLIPIIGWLIII	IFN-γ	2.15.7	Non-toxic
AAO71551.1	RRLPKFGFTSR	MHCI	0.7354	Non-toxic
	VVDLNTLKAANIIG	MHCII	0.5937	Non-toxic
	SGLGKTGGRGHKGQKS	B-cell	2.5383	Non-toxic
	VTVRGLRVTKGARAA	IFN-γ	1.1425	Non-toxic

3.3. Design of immunoinformatics recombinant structure and evaluation of its physicochemical properties

A recombinant vaccine was designed with an N-terminal HBHA adjuvant domain and a C-terminal epitope domain. The epitope domain contained MHC class I/II, B-cell, and IFN-γ-inducing epitopes linked via rigid "KP" peptide linkers. The HBHA and epitope domains were connected by an "EAAAK" rigid linker (Fig. 1).

3.4. Assessment the secondary and tertiary structures

The secondary structure distribution of the engineered recombinant vaccine construct was evaluated using the SOPMA server. Analysis revealed a composition of 50.53 % alpha helix, 8.85 % extended strand, and 40.61 % random coil (Fig. 2). The tertiary structure was predicted using the I-TASSER server and subsequently validated through Ramachandran plot analysis. Initial modeling indicated that 82 %, 12 %, and 1 % of residues resided in the favored, allowed, and outlier regions, respectively. Following structural refinement, these values improved to 91 %, 5 %, and 1 % (Fig. 3). Ramachandran analysis evaluates the dihedral angles (φ and ψ) to determine the geometric quality and stability of protein secondary structures.

3.5. Physicochemical properties, antigenicity, solubility

Physicochemical characterization of the engineered recombinant vaccine construct (655 amino acids) yielded the following properties: molecular weight of 69,846.37 Da, theoretical pI of 9.08, aliphatic index of 66.53, GRAVY index of −0.712, and instability index of 34.22. According to ProtParam algorithms, an instability index below 40 indicates a stable protein, confirming the thermal stability of the construct. The negative GRAVY value (−0.712) suggests a hydrophilic, soluble protein rather than a membrane-associated hydrophobic protein [8]. Antigenicity prediction via VaxiJen server yielded a score of 1.0356. Hydrophobicity analysis using the PEPTIDE 2.0 server showed a composition of 40.31 % hydrophobic, 10.69 % acidic, 18.63 % basic, and 30.38 % neutral residues. The construct exhibits hydrophilic characteristics, as hydrophobic residues constitute < 50 % and charged residues (acidic + basic = 29.32 %) exceed the 25 % threshold associated with hydrophilic peptides. This composition supports solubility in aqueous solutions.

3.6. Immunogenicity of developed recombinant vaccine construct

Immune response simulation for the epitope-based recombinant vaccine construct was performed using the C- ImmSim server. The results demonstrated significant enhancement of both primary and secondary humoral and cellular immune responses. The construct elicited robust production of immunoglobulins, including IgG1, IgG2, and IgM (Fig. 4A). Furthermore, it substantially increased memory B cell populations (Fig. 4B: green, red, and black curves represent memory B cells, IgM, and total B cells, respectively) and active B lymphocytes (Fig. 4C: purple curve indicates active B cell levels).

Cellular immunity analysis revealed elevated levels of key T cell populations. T helper memory lymphocytes (Fig. 5A: black curve compared to right Y-axis show total CD4 + T helper cells), active T lymphocytes (Fig. 5B: purple and red graphs represent active and resting T cells), and regulatory T lymphocytes (Fig. 5C: orange and yellow graphs indicate active and resting regulatory T cells) showed significant increases. Notably, the construct also enhanced active CD8 + T lymphocyte populations. The memory CD8 + cell (on right Y-axis in Fig. 6A) and anergic population (on right Y-axis in Fig. 6B) showed no oscillation along the x-axis.

Concentration (ng/mL on Y-axis) of IFN-γ (purple curve), IL-10 (black curve), IL-12 (blue curve), TGF-β (orange curve), and others cytokines measured over 35 days (X-axis) (Fig. 7). IFN-γ demonstrates early-phase induction with peak response at day 7, and then progressive decline. TGF-β exhibits suitable kinetics with maximal expression at day 14. Inset: Magnified view of initial phase (days 0–10) highlighting transient fluctuations in cytokine concentrations. The critical danger signal 'D' marks the onset of immune activation, coinciding with the earliest detectable cytokine responses.

3.7. Molecular docking and dynamic investigation

Protein-protein docking between the HBHA adjuvant domain and the TLR4/MD2 receptor complex was performed using the ClusPro server (Fig. 8A). The selected model, comprising 42 cluster members, exhibited the lowest binding energy (−1019.1 kcal/mol) and a cluster center score of −935.5. Analysis revealed the formation of multiple hydrogen bonds between the interacting domains (Fig. 8B).

Table 3
BLASTP results for extracted epitopes in different *Salmonella* strains.

Epitopes	Type	*S. Typhi* (TY2)	*S. Enteritidis* (P125109)	*S. Typhimurium* (LT2)	*S. Newport* (SL254)
		Id / E-value	Id / E-value	Id / E-value	Id / E-value
FSHTVGLTY	MHCI	100 % / 0.001	100 % / 0.001	100 % / 0.001	100 % / 0.001
GLSSAAFAA		100 % / 0.001	100 % / 0.001	88.9 % / 0.1	88.9 % / 0.1
NSDITVGQY		100 % / 0.001	100 % / 0.002	100 % / 0.003	100 % / 0.001
KQAEEAAKL		100 % / 0.001	90.9 % / 0.1	81.8 % / 1.0	90.9 % / 0.1
VTNLDFDHY		100 % / 0.001	100 % / 0.001	100 % / 0.001	100 % / 0.001
NRFGPDPKRF		100 % / 0.001	100 % / 0.001	100 % / 0.001	100 % / 0.001
RRLPKFGFTSR		100 % / 0.001	90.9 % / 0.1	81.8 % / 1.0	90.9 % / 0.1
MRFFFILMVLPGADR	MHCII	100 % / 0.001	100 % / 0.001	100 % / 0.001	100 % / 0.001
SAAFAAETATPAKTA		100 % / 0.001	100 % / 0.001	100 % / 0.001	100 % / 0.001
TQNGFRNNATIDQWNA		100 % / 0.001	100 % / 0.001	100 % / 0.001	100 % / 0.001
VQQYNRQQDQQASAR		100 % / 0.001	100 % / 0.001	100 % / 0.001	100 % / 0.001
RWNIHQESTMHAGSG		100 % / 0.001	100 % / 0.001	100 % / 0.001	100 % / 0.001
IIAFNCQNGTPGDNR		100 % / 0.001	100 % / 0.001	100 % / 0.001	100 % / 0.001
VVDLNTLKAANIIG		100 % / 0.001	100 % / 0.001	100 % / 0.001	100 % / 0.001
KEEEKTDKQYDTGHAS	B-cell	100 % / 0.001	100 % / 0.001	100 % / 0.001	100 % / 0.001
EQKAQAAKKHQKKDGK		100 % / 0.001	100 % / 0.001	100 % / 0.001	100 % / 0.001
SETTITQSGYGNGADV		100 % / 0.001	100 % / 0.001	100 % / 0.001	100 % / 0.001
DEHIEASAGGGGGSAI		100 % / 0.001	100 % / 0.001	100 % / 0.001	100 % / 0.001
GGTITAGYDFKANKEI		100 % / 0.001	100 % / 0.001	100 % / 0.001	100 % / 0.001
NCQNGTPGDNRFGPDP		100 % / 0.001	100 % / 0.001	100 % / 0.001	100 % / 0.001
SGLGKTGGRGHKGQKS		100 % / 0.001	100 % / 0.001	100 % / 0.001	100 % / 0.001
GSGWVLQRYYQGEER	IFN-γ	100 % / 0.001	100 % / 0.001	100 % / 0.001	100 % / 0.001
GIKMKKVLALVVAAA		100 % / 0.001	100 % / 0.001	100 % / 0.001	100 % / 0.001
GGGGNHNGGGNSSGP		100 % / 0.001	100 % / 0.001	100 % / 0.001	100 % / 0.001
AAAEAKKKAEAEAAK		100 % / 0.001	100 % / 0.001	100 % / 0.001	100 % / 0.001
STMHAGSGLGSGKVS		100 % / 0.001	100 % / 0.001	100 % / 0.001	100 % / 0.001
LLLLLIPIIGWLIII		100 % / 0.001	100 % / 0.001	100 % / 0.001	100 % / 0.001
VTVRGLRVTKGARAA		100 % / 0.001	100 % / 0.001	100 % / 0.001	100 % / 0.001

Table 4
Population Coverage Analysis.

Population/Area	Class I Coverage	Class II Coverage	Class Combined Coverage
Europe	67.96 %	62.46 %	87.97 %
West Africa	27.18 %	65.52 %	74.89 %
Southwest Asia	39.57 %	55.79 %	73.28 %
South Asia	24.77 %	63.01 %	72.17 %
East Africa	30.68 %	53.44 %	67.72 %
North Africa	38.36 %	46.37 %	66.94 %
Central Africa	16.49 %	44.1 %	53.32 %
East Asia	25.46 %	11.98 %	34.39 %
Northeast Asia	17.91 %	16.59 %	31.53 %
Southeast Asia	17.17 %	15.97 %	30.4 %
South Africa	17.41 %	0.0 %	17.41 %

* The table is sorted based on the data in the 4th column.

The stability of the protein–protein complex was assessed over a 200 ns molecular dynamics (MD) simulation using GROMACS software.

3.8. Root mean square deviation (RMSD) analysis

RMSD analysis of the candidate vaccine in complex with TLR4/MD2 (Fig. 9A) showed major conformational changes: starting at 0.05 nm, it progressively increased to ~ 3.0 nm after initial equilibration (1.3 nm), stabilizing at 2.8–3.0 nm post-116 ns. This indicates significant structural adaptation in the 655-amino acid protein for TLR4/MD2 binding, likely impacting its plasticity. In contrast, the TLR4/MD2 in complex with candidate vaccine (Fig. 9B) exhibited high stability: beginning at 0.2 nm, peaking at 0.38 nm within 10 ns, then stabilizing near 0.25 nm after 45 ns with minimal fluctuation. The protein-TLR complex (Fig. 9C) displayed intermediate dynamics: rapid initial rise to ~ 1.0 nm, fluctuations around 1.4 nm, and final stabilization at 1.2–1.6 nm. The final ~ 1.5 nm RMSD reflects substantial but stable deviation from the initial structure.

3.9. Root mean square fluctuation (RMSF) analysis

The RMSF diagram shows the fluctuation of each amino acid around its average position during the simulation. In the RMSF graph of 655 amino acids of the developed vaccine, most of the amino acids show average RMSF values that vary between 0.5 and 1.5 nm. However, in several regions they show significant high RMSF values, which indicate increased flexibility and mobility, especially in the range of 1–180 and 430–650 residues. These regions are probably related to the loops or the ends of the protein structure. Residues at 180–430 positions usually show lower RMSF values, indicating a more stable region of the protein structure (Fig. 10A). Next, the RMSF of the amino acid residues in the TLR4/MD2 protein during interaction with the developed recombinant construct shows that the majority of the residues have moderate RMSF values, which usually vary between 0.1 nm and 0.2 nm. This suggests that these regions of the protein maintain a relatively stable conformation during the simulation. However, several residues show higher RMSF values, indicating increased flexibility and mobility in the complex. This is particularly noticeable in the regions around residues of 202–201, 266–263, 543–542, and 586–5836, which show RMSF values greater than 0.25 nm, up to a maximum of 0.41 nm in the 612 residues. Increased flexibility in these parts may be very important for protein function and interaction with its binding partner (Fig. 10B).

3.10. Gyration analysis of proteins

Radius of gyration (Rg) which is known as a measurement of the overall compactness of the protein structure, fluctuating over the simulation. For the recombinant vaccine construct in complex with TLR4/MD2, Rg was monitored over a 200 ns simulation (Fig. 11A). Rg values range from approximately 3.30 nm to 4.01 nm, with an average value of 3.85 ± 0.11 nm. The Rg plot (Fig. 11A) exhibits several peaks and troughs, indicating structural changes in the complex throughout the simulation. These fluctuations likely arise from dynamic interactions between the vaccine construct and TLR4/MD2, as well as the intrinsic flexibility of the protein.

Besides, Rg of the TLR4/MD2 protein in complex with the developed

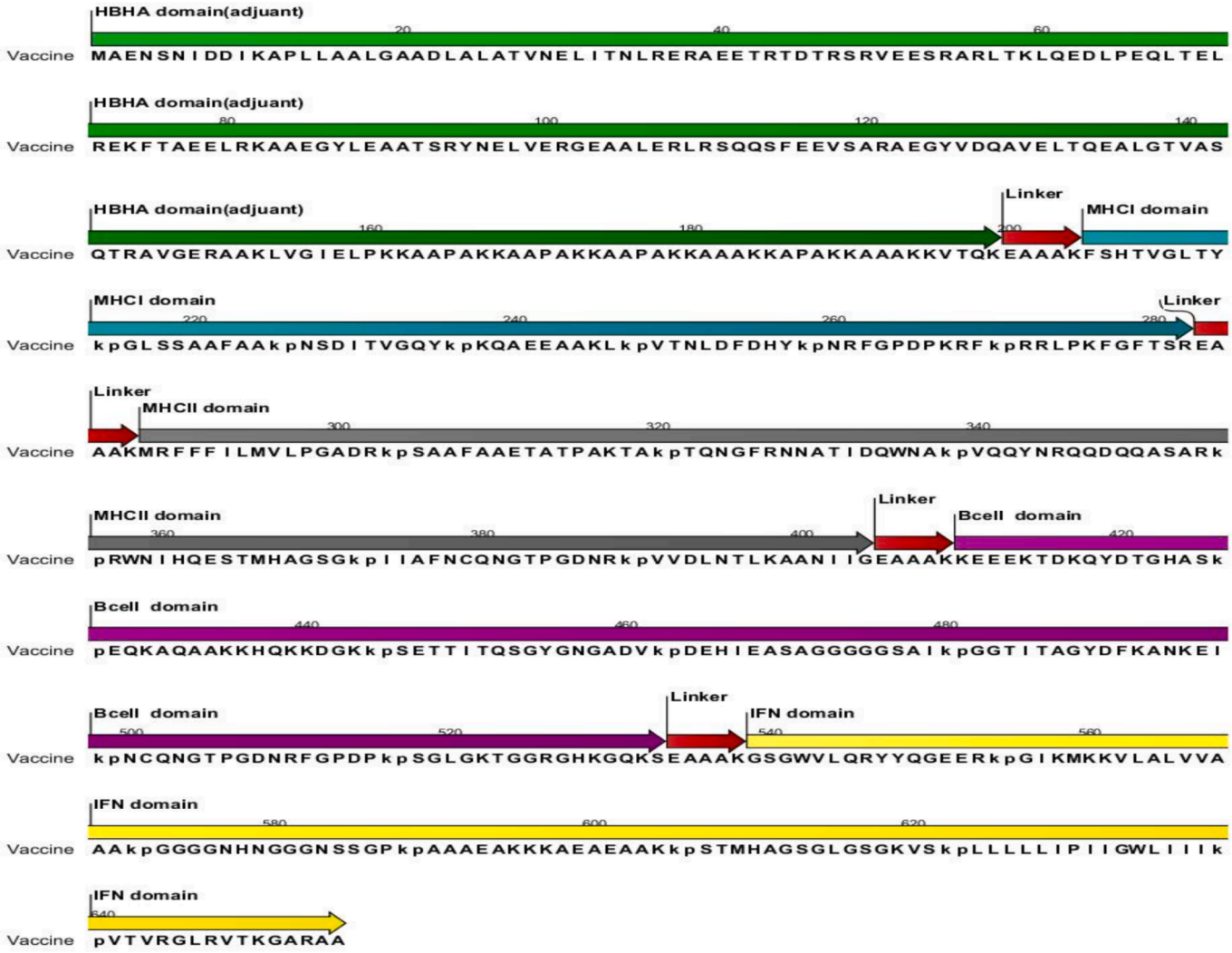

Fig. 1. The developed candidate vaccine comprises five main domains: a molecular adjuvant (green), MHCI epitopes (blue), MHCII epitopes (gray), B-cell epitopes (purple), and IFN-γ epitopes (yellow). Rigid peptide linkers (red) connect these domains.

vaccine protein was investigated during 200 ns molecular dynamics simulation, including a dynamic structural fluctuation during the simulation (Fig. 11B).

The Rg value started at 3.15 nm at the beginning of the simulation and gradually increased, reaching a maximum of 3.32 nm around 1.2 ns. Following this initial adjustment, Rg values stabilized and fluctuated between approximately 3.15 nm and 3.22 nm for the remainder of the simulation (Fig. 11B). This relative stability indicates that the overall size and shape of the TLR4/MD2 complex do not change significantly during the simulation period.

3.11. Hydrogen bond analysis

Hydrogen bond analysis of the recombinant protein-TLR4/MD2 complex was performed successfully over a 200 ns molecular dynamics simulation. Based on the results, the number of hydrogen bonds varies from a minimum of 9 bonds to a maximum of 45 bonds during the simulation. The average number of hydrogen bonds during the simulation was 28 (Fig. 12). The high number of hydrogen bonds consistently observed throughout the simulation trajectory indicates stable interactions between the recombinant protein and TLR4/MD2.

3.12. MM/PBSA binding free energy and per-residue decomposition analysis

To quantify the binding affinity and identify key residues contributing to complex stability, Molecular Mechanics Poisson-Boltzmann Surface Area (MM/PBSA) calculations were performed. This analysis allows us to describe the individual energy contribution of each residue in the protein–ligand complex. By examining residue-specific ΔEGAS, ΔGPOL, and ΔGNP values, residues that significantly contribute to the affinity and overall stability of the complex can be identified. The MM/PBSA decomposition analysis is summarized in Table 5. Average binding free energy (ΔTOTAL) was determined to be −89.15 kcal/mol, with a standard deviation of 7.93 kcal/mol. Regarding the contribution of key energy components; The van der Waals interactions (ΔVDW) was −224.6 kcal/mol, while the electrostatic interactions (ΔELEC) contributed −4696.04 kcal/mol. The solvation free energy (ΔEGB) was 4861.97 kcal/mol, with a gas phase energy (ΔGGAS) contribution of −4920.64 kcal/mol ($\Delta VDW_{+}\Delta ELEC$) and a solvation energy (ΔGSOLV) contribution of 4831.49 kcal/mol. The surface energy (ΔESURF) was found to be −20.48 kcal/mol.

3.13. Per-residue decomposition energy calculations

Residue-specific energy analysis was performed to identify specific

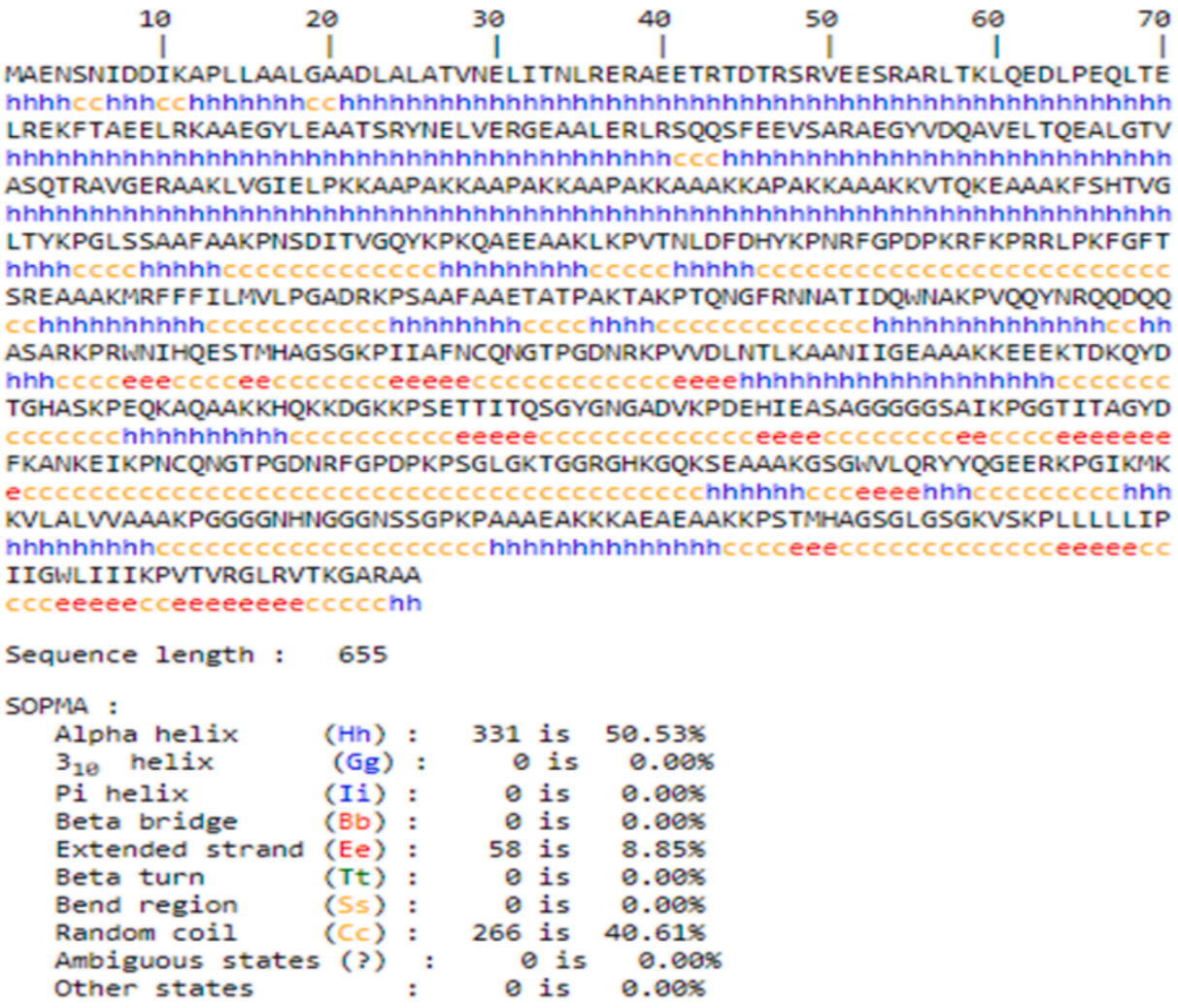

Fig. 2. Distribution of different structural states in the secondary structure of the developed vaccine construct. Blue, red and yellow colors correspond to alpha helix, extended strand and random coil structures, respectively.

A

Statistic	Observed	Expected
Resolution	-	-
R Value	-	-
# res in phipsi core	601 (91%)	590 (90%)
# res in phipsi allowed	38 (5%)	46 (7%)
# res in phipsi generous	7 (1%)	7 (1%)
# res in phipsi outside	9 (1%)	0 (0%)
# res in omega core	638 (97%)	629 (96%)
# res in omega allowed	12 (1%)	20 (3%)
# res in omega generous	2 (0%)	0 (0%)
# res in omega outside	3 (0%)	7 (1%)
# packing defects	306	45
Free energy of folding	-419.14	-632.43
# res 95% buried	113	298
# buried charges	19	0

B

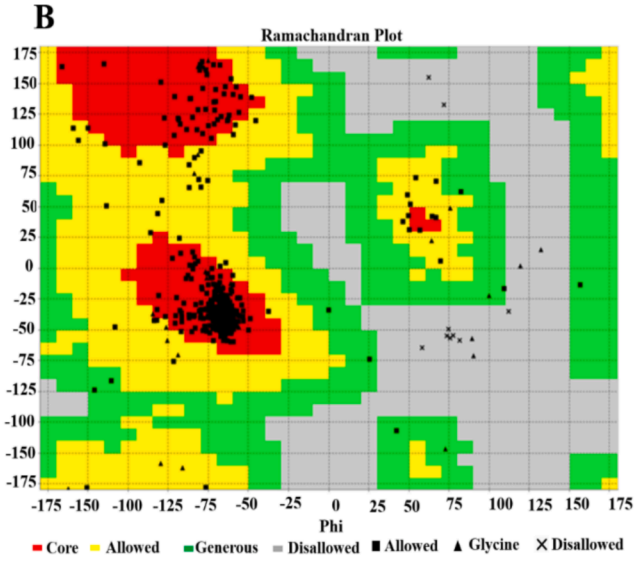

Fig. 3. A: Ramachandran statistical analysis of the best refined 3D model of the developed vaccine structure. B: Ramachandran plot of the best predicted and refined 3D model. Red, yellow, green and grey areas correspond to the core, allowed, acceptable and disallowed regions, respectively. The x-axis and y-axis represent the phi (φ) and the psi (ψ) dihedral angles of amino acid residues in the protein's tertiary structure.

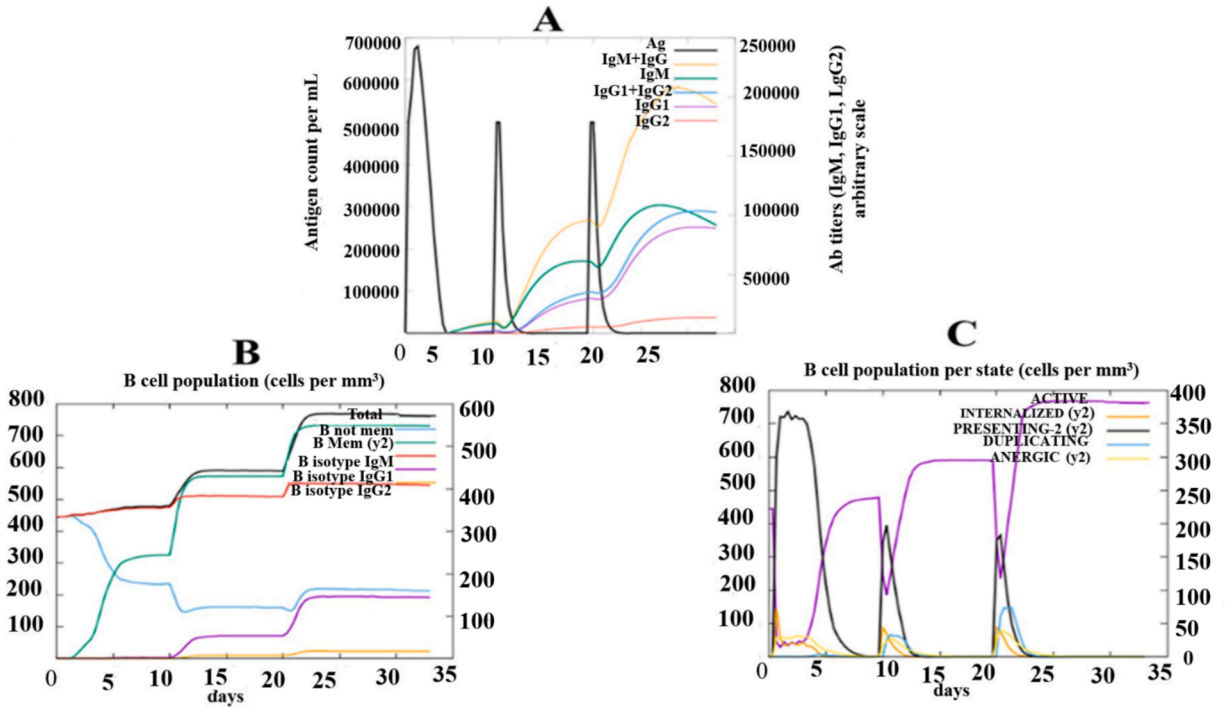

Fig. 4. Simulation of humoral immune response to the candidate vaccine over 35 days (X-axis). A: IgG (blue curve), IgM (green curve) antibody titers and antigen count (black curve compared to left Y-axis) over time, B: Changes in total B cell (black curve compared to left Y-axis), memory B cell (green curve compared to right Y-axis) and IgM isotope titers over time. C: Distribution of B cell activation states: Activated B cells (purple curve compared to left Y-axis), antigen-presenting B cells (black curve compared to right Y-axis), and internalization activity (orange curve, right Y-axis) in response to the vaccine over time.

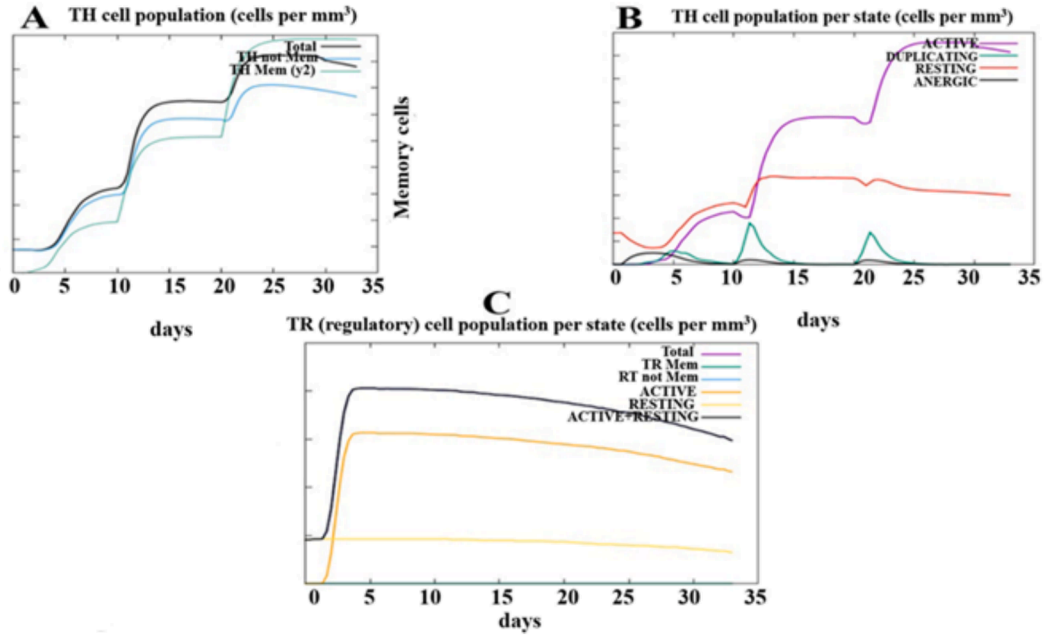

Fig. 5. Simulation of the cellular immune response (lymphocytes with CD4 marker) to the developed candidate vaccine over the 35 days (X-axis). A: Total titer of CD4 T helper lymphocytes (black curve in compare to left axis) and memory T lymphocytes (green graph in compare to right Y-axis) over 35 days. B: Different activation states (active, resting, anergic and duplicating presented with purple, red, black and green colure, respectively). Y-axis represents the cell count and X-axis shows the time. C: Active and resting T regulatory (orange and yellow curves) count (Y-axis) in 35 days (X-axis).

residues that drive affinity at the recombinant protein (R chain)-TLR4/MD2 (L chain) interface. This analysis quantified each residue contribution through internal, van der Waals, electrostatic, polar solvation, and non-polar solvation energy terms (Fig. 13). Residues exhibiting highly favorable energy contributions (negative) were identified as critical for complex stability.

4. Discussion

Salmonella enterica serovar Typhi causes typhoid fever and launches

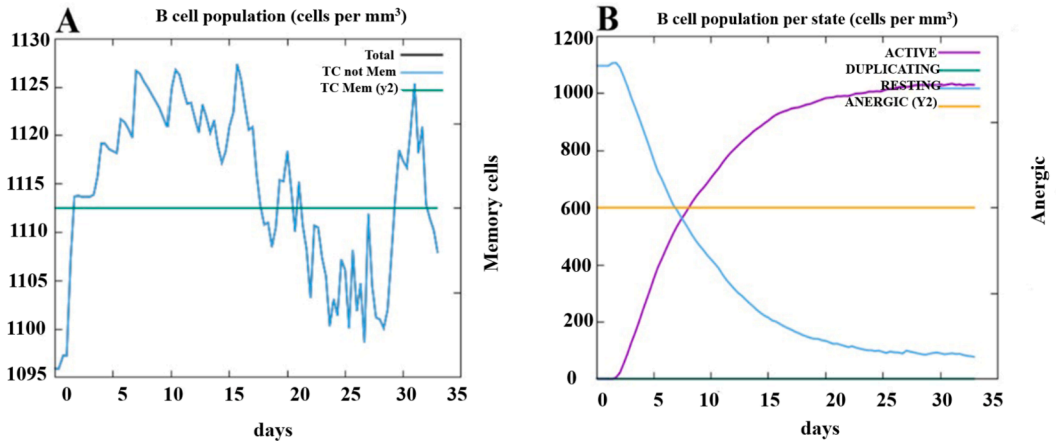

Fig. 6. CD8 + cytotoxic T lymphocyte count in cellular immunity simulation in response to developed candidate vaccine during the time (X-axis). A: Total CD8 + T cell count (cell/mm^3), green and blue curves represent the CD8 + memory T cells count (right Y-axis) and not memory CD8 + T cell count, respectively. B: CD8 + T cell count of different populations; the purple, green, and blue curves show cell counts per mm^3 for active, duplicating, resting populations on left Y-axis and orange curve quantifies the anergic populations on right Y-axis during the 35 days (X-axis).

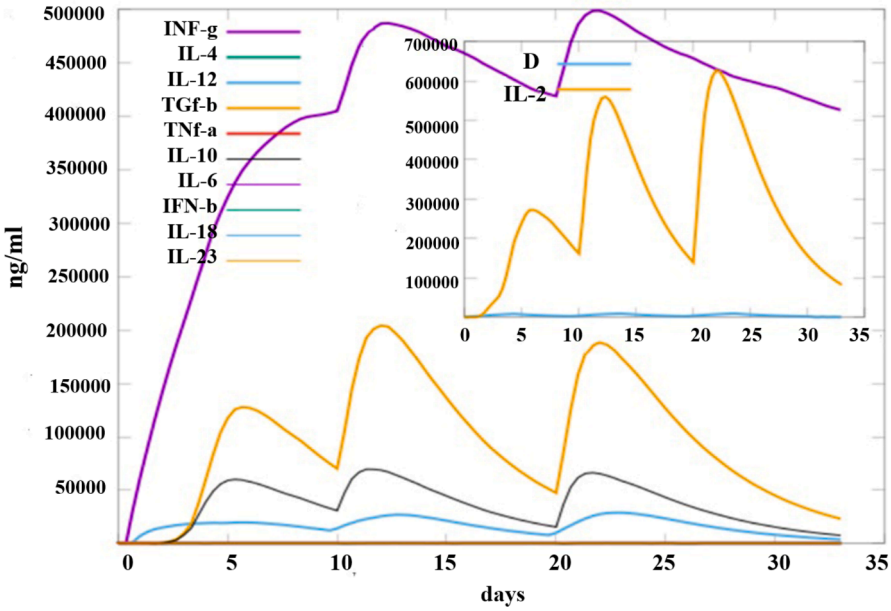

Fig. 7. Spatiotemporal dynamics of cytokine concentrations during immune response progression. Main plot: Time-dependent concentration (ng/mL on Y-axis) of IFN-γ (purple curve), IL-10 (black curve), IL-12 (blue curve), TGF-β (orange curve), and others cytokines measured over 35 days (X-axis). IFN-γ demonstrates early-phase induction with peak response at day 7, followed by progressive decline. TGF-β exhibits suitable kinetics with maximal expression at day 14. Inset: Magnified view of initial phase (days 0–10) highlighting transient fluctuations in cytokine concentrations. The critical danger signal 'D' marks the onset of immune activation, coinciding with the earliest detectable cytokine responses.

both mucosal and systemic immune responses in the host. *Salmonella* Typhi is a facultative intracellular pathogen that induces both humoral and cellular immunity after infection or immunization with live attenuated oral vaccines [13,14]. Like other gastrointestinal pathogens, *salmonella* invades the Peyer's plaques in the ileum wall and stimulates the host's mucosal immunity [15,16]. Based on the studies conducted in typhoid patients, a high titer of all three major classes of immunoglobulin (IgG, IgA and IgM) has been detected [17]. These immunoglobulins were also found in the serum of individuals vaccinated with subunit vaccines containing the Vi antigen of *Salmonella* Typhi, while the antibodies in the serum of those vaccinated with the vaccine containing O antigen were mostly IgA [18,19]. Immune responses against *Salmonella* usually target the O-polysaccharide region of the lipopolysaccharide (LPS) complex of the outer membrane of the *Salmonella* Typhi cell wall. [20]. Therefore, high and rapid secretion of specific antibodies during acute infection requires vaccination with vaccines that induce active humoral immunity and immunological memory. In this study, the results of humoral immune system simulation by the developed vaccine structure showed a significant and favorable level of total antibodies, active antibodies, and memory antibodies in response to the developed vaccine. Furthermore, due to the intracellular nature of *salmonella* Typhi, this pathogen attacks macrophages, dendritic cells and other cells of the immune system to multiply. This intracellular living facilitates bacterial antigen processing and presentation via MHC molecules to T lymphocytes [21]. Th1 lymphocytes, by producing cytokines such as interferon gamma and interleukin-2, play the main role in stimulating immune responses by cytotoxic T cells and macrophages [22]. Gamma interferon secreted by Th1 lymphocytes also induces immunoglobulin class switching towards IgG1 and IgG2a production [23,24]. Therefore, stimulating and creating memory cells is crucial for combating

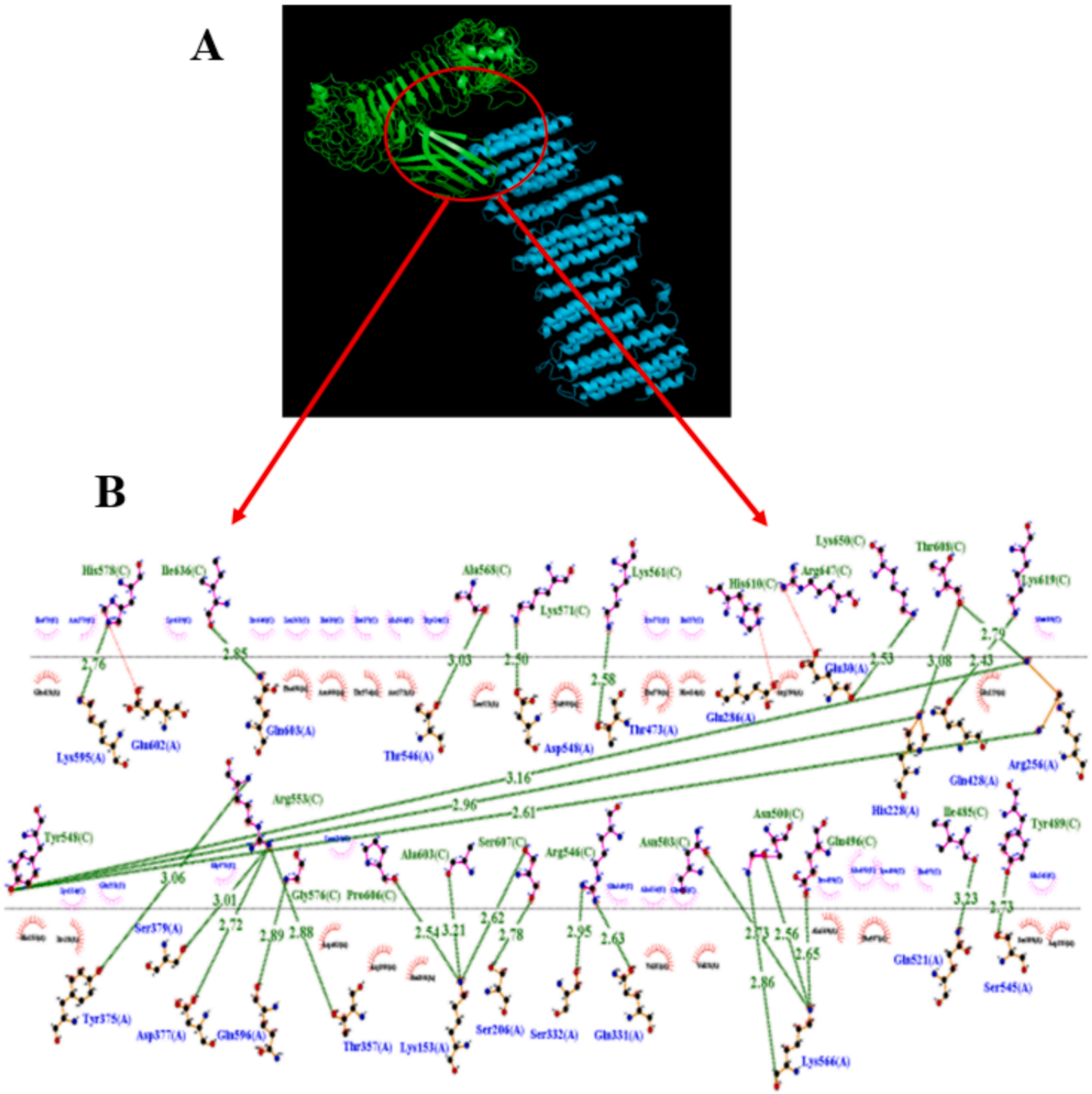

Fig. 8. A: Molecular docking of HBHA (blue) and TLR4 (green). B: LigPlot + visualization of intermolecular bonds between HBHA and TLR4/MD2. Hydrogen and ionic bonds are shown in green and red dashed lines, respectively. Amino acid residues of TLR4 and HBHA proteins are labeled in green and blue colors, respectively.

intracellular pathogens like *Salmonella*. As mentioned in this study, the developed vaccine effectively simulated cellular immunity by successfully inducing the production of both active and memory CD4 + and CD8 + T lymphocytes. In addition, the significant increase in IFN-γ, IL-2 and TGF-β secretion was also observed in a stimulation period. The candidate vaccine consisted of epitope and adjuvant domains. Specialized epitopes from MHCI, MHCII, B cell and IFN-γ molecules, derived from seven immunogenic proteins identified through whole proteome screening, were linked together through a rigid linker "KP". This domain was linked to the HBHA protein using a peptide linker "EAAAK". Studies have shown that HBHA protein as a TLR4/MD2 receptor agonist without systemic toxicity, stimulates the maturation of dendritic cells, secretion of IFN-γ and T cell-mediated cellular cytotoxicity [25]. The use of HBHA molecule in the design of second-generation subunit vaccines to deal with a diverse pathogen has been highly regarded and proven [3,26–28], so it can be considered as a valuable molecular adjuvant. Linkers also play a key role in the biological function of a structure composed of multiple protein domains. EAAAK (which has an alpha-helical structure) and KP peptides create rigid connections between domains, which are usually important for maintaining structural integrity and function of a multi-domain structure. [29].

In the present study, the investigation of different secondary structures in the developed vaccine showed a significant promotion of random coil structures, these conformations are essential for ligand binding due to their exposed hydrophilic regions, and a high random coil content typically indicates antigenic potential [30]. In addition, it

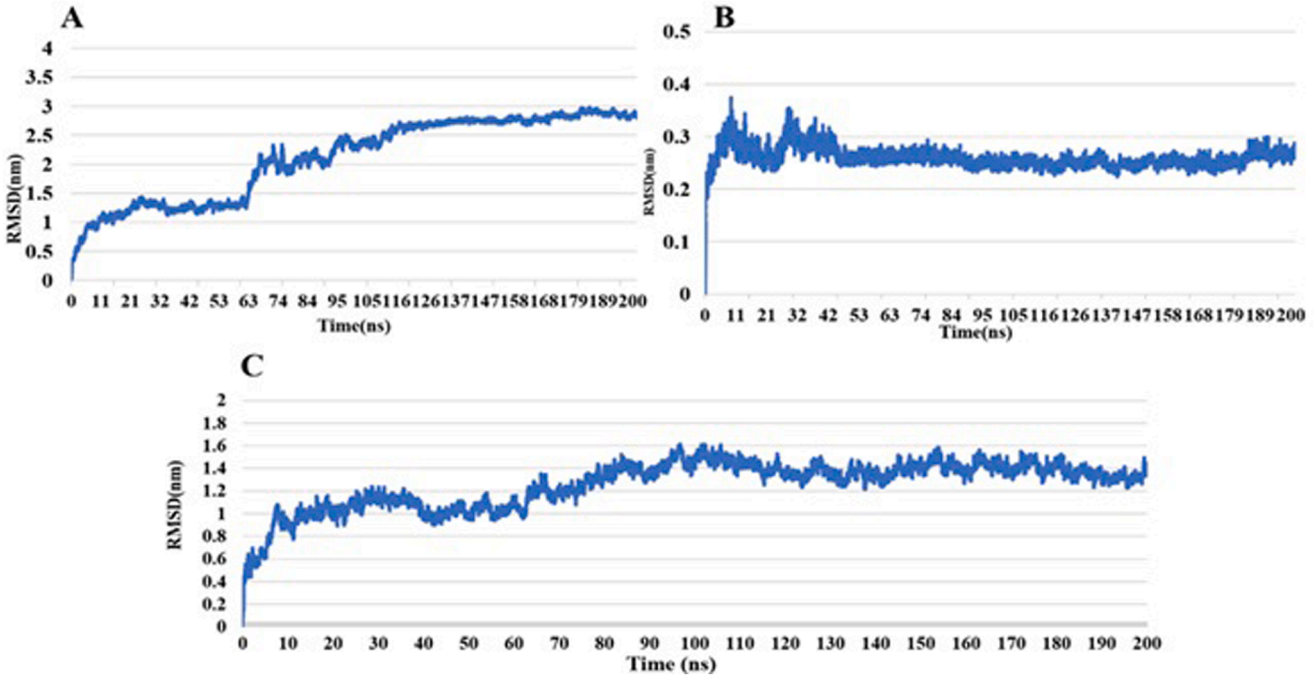

Fig. 9. Root mean square deviation (RMSD) analysis of the protein-TLR4 complex during molecular dynamics simulation. RMSD of the protein backbone (A), RMSD of TLR4 (B) and RMSD of complex (vaccine-TLR4) (C) plotted as a function of simulation time over 200 ns. The x-axis represents simulation time (ns), while the y-axis shows RMSD values (nm). The graphs show the structural-morphological dynamics of the complex during the simulation period, which shows an initial equilibrium followed by stabilization in both components.

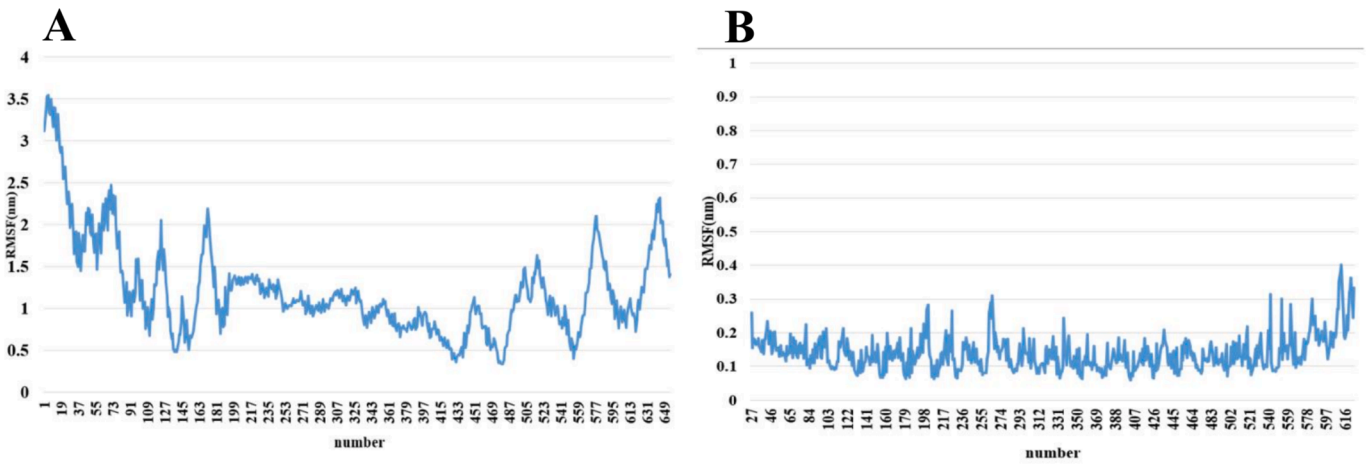

Fig. 10. Root mean square fluctuation (RMSF) analysis of the developed vaccine −TLR4 complex. A: RMSF values for each amino acid residue in the vaccine construct. B: RMSF values for each amino acid residue in TLR4 during 200 ns molecular dynamics simulation. The x-axis represents the amino acid residue number, while the y-axis shows RMSF values (nm). Higher RMSF values indicate regions of greater flexibility and conformational mobility, which are often associated with functional domains and interaction interfaces.

was found that the isoelectric point of the developed vaccine structure is 9.83, which theoretically is the pH at which the molecule does not carry any electric charge. pI affects the behavior of amino acids in solutions and protein structure, and due to the combined pI of all its amino acids residues, it affects protein stability and function [31]. The aliphatic index (AI) quantifies the relative volume occupied by aliphatic side chains (alanine, valine, leucine, and isoleucine) within a protein. The aliphatic index plays a role in the thermal stability of the protein. proteins with high aliphatic indices exhibit greater thermal stability, as aliphatic amino acids are inherently hydrophobic [31,32]. In this study, the aliphatic index of the recombinant structure was 53.66, indicating protein stability during a wide temperature range. In addition, the GRAVY (Grand Average of Hydropathy) value for a peptide or protein is calculated as the sum of the hydropathy values of all amino acids divided by the number of residues [31]. Our recombinant structure demonstrated a GRAVY index of −0.712. suggesting a hydrophilic, soluble conformation rather than a hydrophobic membrane-associated state, a property relevant to protein localization [33]. Also, the developed structure was predicted to be a non-allergenic protein with a favorable antigenicity score of 1.0356. Generally, antigenicity refers to the ability of a structure to elicit normal immune system responses, while allergenicity refers to the ability of a structure that launches harmful abnormal immune responses resulting in serious harm to the host [34]. Further, the predicted instability index for this recombinant structure was calculated to be less than 40, confirming protein stability [35]. In this study, the molecular docking process was employed to

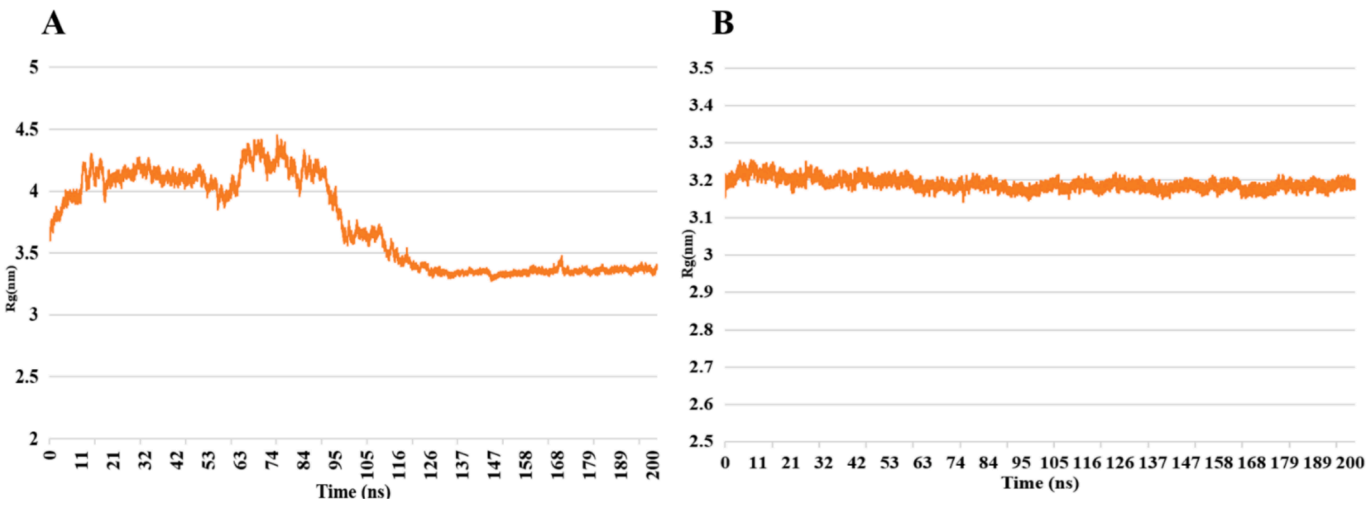

Fig. 11. A: Gyrate radius (Rg) plot of the recombinant vaccine structure in complex with TLR4. B: Gyrate radius (Rg) plot of TLR4 protein in complex with the recombinant vaccine structure during 200 ns molecular dynamics simulation. The x and y axes represent gyrate (nm) and the time of the trajectory (ns), respectively.

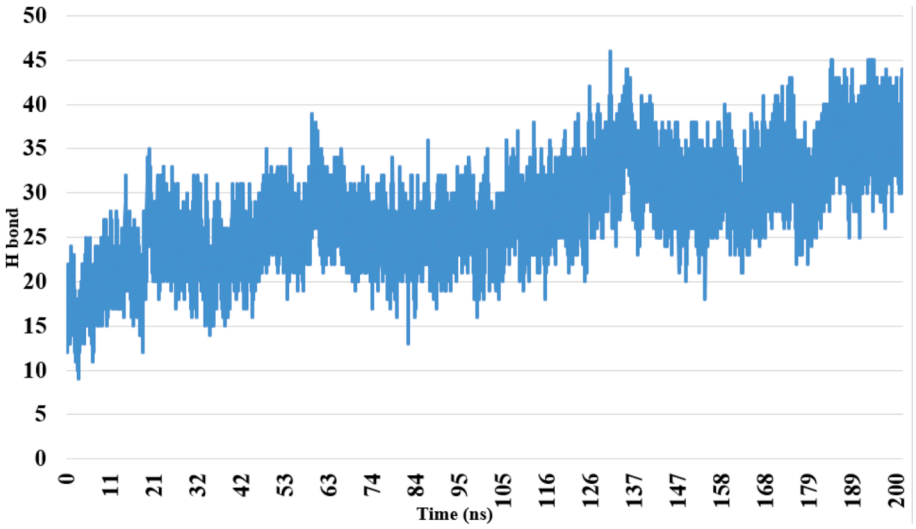

Fig. 12. Hydrogen bond diagram of the protein-TLR4 complex in 200 ns molecular dynamics simulation. The x and y axes represent number of hydrogen bonds during the simulation and the time of the trajectory (200 ns), respectively.

Table 5
Calculated binding free energy from MM/PBSA analysis.

Energy Terms	Average (kcal/mol)	Standard Deviation (kcal/mol)
ΔVDW	−224.6	7.94
ΔELEC	−4696.04	81.91
ΔEGB	4861.97	84.73
ΔESURF	−20.48	1.06
ΔGGAS	−4920.64	86.64
ΔGSOLV	4831.49	84.02
ΔTOTAL	−89.15	7.93

The analysis considered various energy terms, including ΔVDWAALS (van der Waals interactions), ΔEEL (electrostatic interactions), ΔEGB (solvation free energy), ΔESURF (surface energy), ΔGGAS (gas phase energy), ΔGSOLV (solvation energy), and ΔTOTAL (total energy).

investigate the interactions between the HBHA and TLR4/MD2 protein domains. In the docking process, the ligand randomly explores ligand position on a macromolecule with specific algorithms, to find an optimal binding conformation and identify and introduce complexes of the ligand-receptor complex with minimum energy in the active site. [36]. This static analysis occurs in a simplified environment devoid of physiological factors like water molecules, pH variations, and ionic influences. The domains were able to create a stable interaction mediated by several hydrogen bonds. To comprehensively evaluate stability, molecular dynamics simulations assessed the vaccine-TLR4/MD2 complex and individual domains using RMSD, RMSF, radius of gyration, hydrogen bond analysis, and MM/PBSA calculations.

Based on the results the multidomain protein vaccine including the adjuvant-epitope structure achieved a moderate structural stability within 200 ns. The RMSD plot indicates that the overall protein structure stabilized in the range of 2.5–3.0 nm after 116 ns. In parallel, RMSD of complex (vaccine-TLR4) showed moderate stability, reaching a final RMSD of about 1.5 nm with fluctuations of about 1.4 nm, indicating a significant but stable structural deviation. This value corresponds to the stability threshold for large protein complexes and is in good agreement with the stability threshold for protein-receptor complexes in subunit vaccines (RMSD < 3.0 nm) [37]. This stability is enhanced by an increase in hydrogen bonds from 25 to 45 during the simulation, reflecting the strengthening of intramolecular interactions and the system reaching dynamic equilibrium [38,39]. The increase in hydrogen bonds coincides with the stabilization of RMSD in the final stages, indicating structural adaptation. The observed fluctuations in the RMSF of the

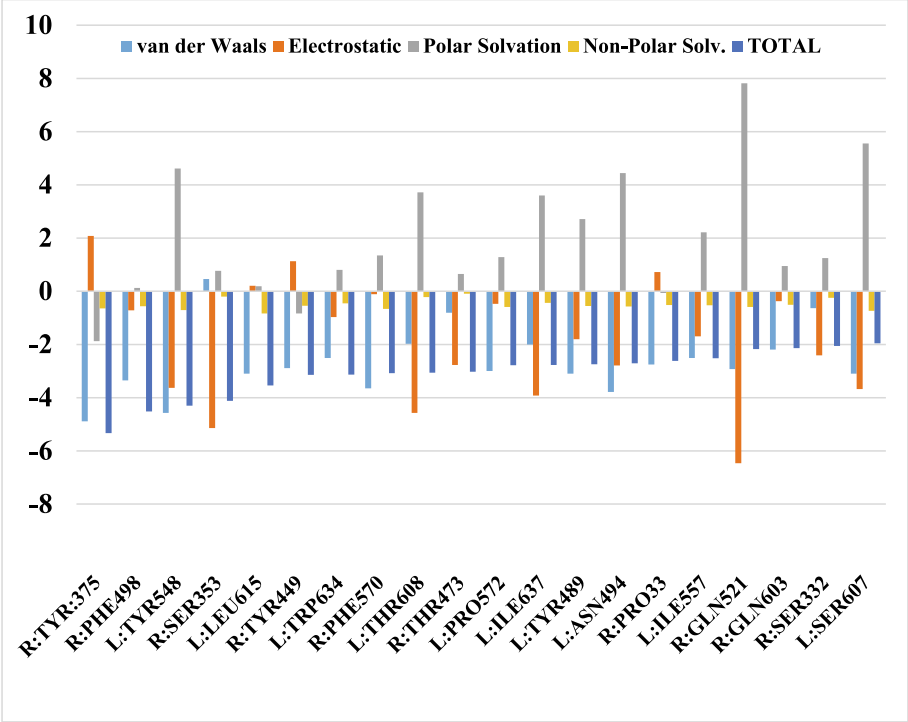

Fig. 13. Energetic decomposition of key residues in the recombinant protein (R chain)-TLR4/MD2 (L chain) interface. Total (ΔGTOTAL) and component (ΔGVDW, ΔGELEC, ΔGPOL, ΔGnp) binding free energies are shown for residues with large interactions.

adjuvant domain (amino acids 1–200) occur alongside the preservation of secondary structure and the increase in hydrogen bonds, suggesting functional flexibility without structural degradation. This pattern is consistent with previous studies on multidomain protein vaccines, where limited fluctuations in the adjuvant domains (up to 1.5 nm) are considered a desirable feature for stimulating an immune response [26,37]. Furthermore, RMSF fluctuations in the adjuvant domain can be explained by the need for this domain to be flexible when interacting with its receptors, as controlled flexibility in this region is essential for binding to receptors such as TLRs [40]. In contrast, the epitope domain exhibits RMSF values below 1.5 nm, which supports the maintenance of a stable secondary structure in this region. The developed candidate vaccine also induced both primary and secondary humoral and cellular immune response. The power, precision, and importance of bioinformatics tools in analyzing the genomic and proteomic data have generated significant research interest. For example, in 2024, Forouharmehr used bioinformatics approaches to design and evaluate a novel epitope-based vaccine against *Coxiella Burnetii* by screening the whole proteome. This candidate vaccine, combining epitope domains with HBHA protein, underwent comprehensive immunoinformatics investigations. At the end of the evaluations, it was determined that the designed recombinant structure had stability, hydrophilicity, antigenicity, non-allergenicity, and affinity for the TLR4/MD2 receptor properties. Furthermore, molecular dynamics simulations confirmed the structural stability of the designed recombinant construct in 200 ns MD trajectories [26]. Immunoinformatics approaches for identifying *Salmonella* vaccine candidates have previously attracted the researchers' interests. In 2022, Zafar et al. introduced a multi-epitope vaccine targeting *Salmonella* Typhimurium using advanced immunoinformatics tools. Their analysis of the *Salmonella* Typhimurium genome identified TolA as a target antigen, from which they predicted optimal CTL and HTL-specific epitopes. Comprehensive bioinformatics evaluation confirmed the recombinant vaccine construct's antigenicity, immunogenicity, and stable binding to immune cell receptors (e.g., TLR4). Simulation results indicated favorable immune system activation, supporting the vaccine's potential immunogenicity [41]. In 2019, Samikan et al. developed and bioinformatically analyzed a subunit vaccine consisting of B-cell and T-cell epitopes derived from the outer membrane peptide of protease E (PgtE) against *Salmonella* Typhi. Their analysis demonstrated stable binding of this recombinant construct to specific HLA alleles associated with typhoid. Molecular dynamics simulation confirmed the stability of the recombinant structure and minimal changes in the radius of gyration. These reports identified this recombinant construct as a promising candidate for typhoid vaccine development. [42]. In another immunoinformatics study in 2019, Shams et al. designed an epitope-based vaccine structure against *Salmonella* Typhi using OmpA, OmpC, and OmpF antigens. Comprehensive evaluation of its physicochemical properties and computational stability assessments (both static and dynamic) identified this construct as a promising candidate against typhoid (28). In total, these studies validate and emphasize the importance of the bioinformatics approaches employed in present study. While experimental validation is necessary, the vaccine designed in this study intentionally has features that make it suitable for in vitro and in vivo applications: low-cost bacterial production, inherent stability over a wide temperature range, and compatibility with existing adjuvants. These features make it a logical candidate for use in typhoid endemic areas where cold chain implementation and cost-effectiveness are major challenges.

5. Conclusion

In the present study, to develop a recombinant and safe vaccine against typhoid fever, we evaluated the entire *Salmonella* Typhi proteome. Among 4,322 proteins, we selected 7 non-allergenic proteins with the highest antigenic scores and predicted their optimal epitopes using reliable immunoinformatics algorithms. We designed a construct combining these specific epitopes with a molecular adjuvant. Immunoinformatics analyses confirmed that this 655-amino acid recombinant vaccine construct exhibits a hydrophilic, stable, antigenic, and non-allergenic profile. The construct demonstrated stability throughout 200 ns molecular dynamics simulations and showed potential to stimulate both humoral and cellular immune responses in silico. Our computational analyses identify this candidate as a promising typhoid

fever vaccine warranting immediate experimental validation. While the integrated immunoinformatics pipeline provides strong theoretical support, experimental studies must confirm: (i) true immunogenicity in biological systems, (ii) structural accessibility of predicted epitopes, and (iii) protective efficacy in challenge models. The proposed tiered validation framework outlines a clear path to translate computational predictions into testable hypotheses. Until experimentally validated, this candidate should be considered a high-priority target for further investigation rather than a proven vaccine.

Ethics statement.

The authors of this article declare that no human or animal was directly or indirectly used in the preparation of this manuscript.

Consent for publication.

The authors of this article declare that there is no applicable.

CRediT authorship contribution statement

Mahsa Beyranvand: Software, Methodology. **Nemat Shams:** Validation, Supervision. **Amin Jaydari:** Visualization, Software. **Narges Nazifi:** Writing – original draft, Methodology, Investigation, Conceptualization. **Peyman Khademi:** Validation.

Funding

This work was supported by the Lorestan university, Khorram Abad, Iran [grant numbers:1402/544.

Declaration of competing interest

The authors declare that they have no known competing financial interests or personal relationships that could have appeared to influence the work reported in this paper.

References

[1] G.C. Buckle, C.L.F. Walker, R.E. Black, Typhoid fever and paratyphoid fever: Systematic review to estimate global morbidity and mortality for 2010, J. Glob. Health 2 (2012).
[2] J.A. Crump, S.P. Luby, E.D. Mintz, The global burden of typhoid fever, Bull. World Health Organ. 82 (2004) 346.
[3] A. Jaydari, N. Nazifi, A. Forouharmehr, Computational design of a novel multi-epitope vaccine against Coxiella burnetii, Hum. Immunol. 81 (2020) 596.
[4] M.M. Levine, J.E. Galen, M.F. Pasetti, M.B. Sztein, Attenuated strains of Salmonella enterica serovars Typhi and Paratyphi as live oral vaccines against enteric fever, CRC Press, New generation vaccines, 2016, p. 525.
[5] K.A. Syed, T. Saluja, H. Cho, A. Hsiao, H. Shaikh, T.A. Wartel, et al., Review on the recent advances on typhoid vaccine development and challenges ahead, Clin. Infect. Dis. 71 (2020) S141.
[6] K. Wong, J.C. Feeley, Isolation of Vi antigen and a simple method for its measurement, Appl. Microbiol. 24 (1972) 628.
[7] Organization WH: Typhoid vaccines: WHO position paper. Weekly Epidemiological Record= Relevé épidémiologique hebdomadaire 2008;83:49.
[8] S. Wold, J. Jonsson, M. Sjörström, M. Sandberg, S. Rännar, DNA and peptide sequences and chemical processes multivariately modelled by principal component analysis and partial least-squares projections to latent structures, Anal. Chim. Acta 277 (1993) 239.
[9] Q. Zhang, P. Wang, Y. Kim, P. Haste-Andersen, J. Beaver, P.E. Bourne, et al., Immune epitope database analysis resource (IEDB-AR), Nucleic Acids Res. 36 (2008) W513.
[10] R. Vita, S. Mahajan, J.A. Overton, S.K. Dhanda, S. Martini, J.R. Cantrell, et al., The immune epitope database (IEDB): 2018 update, Nucleic Acids Res. 47 (2019) D339.
[11] J.N. Clifford, M.H. Høie, S. Deleuran, B. Peters, M. Nielsen, P. Marcatili, BepiPred-3.0: improved B-cell epitope prediction using protein language models, Protein Sci. 31 (2022) e4497.
[12] S.K. Dhanda, P. Vir, G.P. Raghava, Designing of interferon-gamma inducing MHC class-II binders, Biol. Direct 8 (2013) 30.
[13] B.D. Forrest, Indirect measurement of intestinal immune responses to an orally administered attenuated bacterial vaccine, Infect. Immun. 60 (1992) 2023.
[14] J.R. McGhee, H. Kiyono, New perspectives in vaccine development: mucosal immunity to infections, Infect. Agents Dis. 2 (1993) 55.
[15] J.F. Prescott, J.I. MacInnes, F. Van Immerseel, J.D. Boyce, A.N. Rycroft, J. A. Vázquez-Boland, Pathogenesis of bacterial infections in animals. Wiley Online, Library (2022).
[16] P. Michetti, M. Mahan, J. Slauch, J. Mekalanos, M. Neutra, Monoclonal secretory immunoglobulin a protects mice against oral challenge with the invasive pathogen Salmonella typhimurium, Infect. Immun. 60 (1992) 1786.
[17] H.I. Shaheen, N.I. Girgis, G.R. Rodier, K.A. Kamal, Evaluation of the Response of Human Humoral Antibodies to Salmonella typhi Lipopolysaccharide in an Area of Endemic Typhoid fever, Clin. Infect. Dis. 21 (1995) 1012.
[18] S. Baker, Y. Sarwar, H. Aziz, A. Haque, A. Ali, G. Dougan, et al., Detection of Vi-negative Salmonella enterica serovar typhi in the peripheral blood of patients with typhoid fever in the Faisalabad region of Pakistan, J. Clin. Microbiol. 43 (2005) 4418.
[19] C. Janis, A.J. Grant, T.J. McKinley, F.J. Morgan, V.F. John, J. Houghton, et al., In vivo regulation of the Vi antigen in Salmonella and induction of immune responses with an in vivo-inducible promoter, Infect. Immun. 79 (2011) 2481.
[20] R. Germanier, E. Fiirer, Isolation and characterization of Gal E mutant Ty 21a of Salmonella typhi: a candidate strain for a live, oral typhoid vaccine, J. Infect. Dis. 131 (1975) 553.
[21] B. Raupach, S.H. Kaufmann, Immune responses to intracellular bacteria, Curr. Opin. Immunol. 13 (2001) 417.
[22] E. Gutiérrez-Martínez, R. Planès, G. Anselmi, M. Reynolds, S. Menezes, A.C. Adiko, et al., Cross-presentation of cell-associated antigens by MHC class I in dendritic cell subsets, Front. Immunol. 6 (2015) 363.
[23] N. Nazifi, M. Tahmoorespur, M.H. Sekhavati, A. Haghparast, A.M. Behroozikhah, In vivo immunogenicity assessment and vaccine efficacy evaluation of a chimeric tandem repeat of epitopic region of OMP31 antigen fused to interleukin 2 (IL-2) against Brucella melitensis in BALB/c mice, BMC Vet. Res. 15 (2019) 1.
[24] L. Rogge, A genomic view of helper T cell subsets, Ann. N. Y. Acad. Sci. 975 (2002) 57.
[25] Y. Lei, J. Shao, F. Ma, C. Lei, H. Chang, Y. Zhang, Enhanced efficacy of a multi-epitope vaccine for type a and O foot-and-mouth disease virus by fusing multiple epitopes with Mycobacterium tuberculosis heparin-binding hemagglutinin (HBHA), a novel TLR4 agonist, Mol. Immunol. 121 (2020) 118.
[26] A. Forouharmehr, Whole proteome screening to develop a potent epitope-based vaccine against Coxiella burnetii: a reverse vaccinology approach, J. Biomol. Struct. Dyn. 1 (2024).
[27] E. Rashidian, Z.S. Gandabeh, A. Forouharmehr, N. Nazifi, N. Shams, A. Jaydari, Immunoinformatics approach to engineer a potent poly-epitope fusion protein vaccine against Coxiella burnetii, Int. J. Pept. Res. Ther. 26 (2020) 2191.
[28] N. Shams, Z. Shakarami Gandabeh, N. Nazifi, A. Forouharmehr, A. Jaydari, E. Rashidian, Computational design of different epitope-based vaccines against Salmonella typhi, Int. J. Pept. Res. Ther. 26 (2020) 1527.
[29] X. Chen, J.L. Zaro, W.-C. Shen, Fusion protein linkers: property, design and functionality, Adv. Drug Deliv. Rev. 65 (2013) 1357.
[30] Y. Li, X. Liu, Y. Zhu, X. Zhou, C. Cao, X. Hu, et al., Bioinformatic prediction of epitopes in the Emy162 antigen of Echinococcus multilocularis, Exp. Ther. Med. 6 (2013) 335.
[31] D. Walker, Oral mucosal immunology: an overview, Annals-Academy of Medicine Singapore 33 (2004) 27.
[32] A. Ikai, Thermostability and aliphatic index of globular proteins, The Journal of Biochemistry 88 (1980) 1895.
[33] S. Enany, Structural and functional analysis of hypothetical and conserved proteins of Clostridium tetani, J. Infect. Public Health 7 (2014) 296.
[34] Zhang J, Tao A: Antigenicity, immunogenicity, allergenicity. Allergy bioinformatics 2015:175.
[35] A. Forouharmehr, M. Nassiri, S. Ghovvati, A. Javadmanesh, Evaluation of different signal peptides for secretory production of recombinant bovine pancreatic ribonuclease a in gram negative bacterial system: an in silico study, Curr. Proteomics 15 (2018) 24.
[36] M.M. Ranjbar, V. Assadolahi, M. Yazdani, D. Nikaein, B. Rashidieh, Virtual dual inhibition of COX-2/5-LOX enzymes based on binding properties of alpha-amyrins, the anti-inflammatory compound as a promising anti-cancer drug, EXCLI J. 15 (2016) 238.
[37] A.T. Moin, R.B. Patil, T. Tabassum, Y. Araf, M.A. Ullah, H.J. Snigdha, et al., Immunoinformatics approach to design novel subunit vaccine against the Epstein-Barr virus, Microbiol. Spectrum 10 (2022) e01151.
[38] I. Chikalov, P. Yao, M. Moshkov, J.-C. Latombe, Learning probabilistic models of hydrogen bond stability from molecular dynamics simulation trajectories, BMC Bioinf. 12 (2011) S34.
[39] L. Zhang, Y. Ding, The relation between lipase thermostability and dynamics of hydrogen bond and hydrogen bond network based on long time molecular dynamics simulation, Protein Pept. Lett. 24 (2017) 643.
[40] S.-i. Yoon, O. Kurnasov, V. Natarajan, M. Hong, A.V. Gudkov, A.L. Osterman, et al., Structural basis of TLR5-flagellin recognition and signaling, Science 335 (2012) 859.
[41] S. Zafar, H. Ajab, S. Baig, A. Baig, Z. Habib, F. Jamil, et al., Prediction and evaluation of multi epitope based sub-unit vaccine against Salmonella typhimurium, Saudi Journal of Biological Sciences 29 (2022) 1092.
[42] G. Samykannu, P. Vijayababu, C.B. Antonyraj, P. Perumal, S. Narayanan, S. I. Basheer Ahamed, et al., In silico characterization of B cell and T cell epitopes for subunit vaccine design of Salmonella typhi PgtE: a molecular dynamics simulation approach, J. Comput. Biol. 26 (2019) 105.